Journal of Photochemistry & Photobiology, A: Chemistry 436 (2023) 114376

Contents lists available at ScienceDirect

Journal of Photochemistry & Photobiology, A: Chemistry

journal homepage: www.elsevier.com/locate/jphotochem

Ternary silver tungstate-MoS_2/graphene oxide heterostructure nanocomposite for enhanced photocatalysis under visible light and antibacterial activity

Noor Tahir [a], Muhammad Zahid [a,*], Asim Jillani [b], Muhammad Yaseen [c], Qamar Abbas [d,e], Rana Abdul shakoor [f], Imran shahid [g,*]

[a] Department of Chemistry, University of Agriculture, Faisalabad 38040, Pakistan
[b] Center of Nanotechnology, King Abdulaziz University, Jeddah, Saudi Arabia
[c] Department of Physics, University of Agriculture Faisalabad, Pakistan
[d] Institute for Chemistry and Technology of Materials, Graz University of Technology, Stremayrgasse 9, Graz 8010, Austria
[e] Institute of Chemistry and Technical Electrochemistry, Faculty of Chemical Technology, Poznan University of Technology, Poznan 60-965, Poland
[f] Center for Advanced Materials (CAM), Qatar University, P.O. Box 2713, Doha, Qatar
[g] Environmental Science Centre, Qatar University, P.O. Box 2713, Doha, Qatar

ARTICLE INFO

Keywords:
Metal tungstates
Wastewater treatment
Metal chalcogenides, Ternary heterojunction
Biological activities

ABSTRACT

Wastewater emanating out of industrial units is loaded with hazardous organic dyes. The hindrance in sunlight penetration into the water by this dye-loaded wastewater has led to disruption in an aquatic ecosystem. Along with these carcinogenic pollutants, biological pollutants such as noxious bacteria are present in wastewater posing serious health problems. Fabrication of narrow bandgap visible light active photocatalysts is crucial these days. Metal tungstates and metal sulphides are mainly being sought due to their unique tailorable optical and chemical properties. In the present study, silver tungstate-MoS_2 supported on graphene oxide was synthesized utilizing the ultrasonic-assisted hydrothermal method. The as-synthesized ternary nanocomposite was characterized by XRD, FTIR, SEM-EDS, TEM, XPS, BET, PL, and UV-vis techniques. The photocatalytic activity of prepared nanocomposites was evaluated using methyl orange degradation under visible light. The ternary nanocomposite showed improved photoefficiency, attaining 93 % methyl orange degradation in 90 min under various optimized conditions of solution pH = 5, initial dye concentration of 10 ppm, and catalyst dose of 50 mg/100 ml. The modelization and optimization for assessing the interaction effect amongst several variables were evaluated employing Response Surface Methodology (RSM). The antibacterial activity of synthesized binary and ternary hybrid nanocomposites was determined by the inactivation of gram-negative (Escherichia coli) and gram-positive (Staphylococcus aureus) bacteria. The improved photocatalytic and antimicrobial activities of ternary nanocomposite may be credited to the synergistic effect of heterojunction among three components.

1. Introduction

Water contamination is caused by tones of organic pollutants particularly various harmful dyes released from industrial units like textiles, pharmaceuticals, paper, and the leather industry. Textile dyes are amongst the most recalcitrant pollutants which are resistant to degradation posing various health hazards to living beings. Along with these organic pollutants, several waterborne pathogens are hazardous to human health and are responsible for spreading various infectious diseases like cholera, typhoid, and diarrhea [60]. Hence, it is highly desirable to synthesize effective heterogeneous systems based on environmentally friendly semiconductor materials that could harness sunlight effectively for the eradication of dyes and noxious bacteria from wastewater [61].

The numerous traditional wastewater treatment technologies for the removal of pollutants and disinfection for the eradication of pathogenic bacteria include chlorination, ozonation, and UV irradiation. However, these processes usually lead to harmful by-products generation, excessive consumption of energy, and incomplete disinfection of water. In heterogeneous photocatalysis based on semiconductor metal oxides and

* Corresponding authors at: Environmental Science Centre, Qatar University, P.O. Box 2713, Doha, Qatar (I. shahid).
E-mail addresses: rmzahid@uaf.edu.pk (M. Zahid), ishahid@qu.edu.qa (I. shahid).

https://doi.org/10.1016/j.jphotochem.2022.114376
Received 29 August 2022; Received in revised form 18 October 2022; Accepted 25 October 2022
Available online 29 October 2022
1010-6030/© 2022 The Author(s). Published by Elsevier B.V. This is an open access article under the CC BY license (http://creativecommons.org/licenses/by/4.0/).

metal dichalcogenides, photocatalyst absorbs sunlight from a visible spectrum having energy equal to or higher than its bandgap and excites electrons from the valence band (VB) to the conduction band (CB). This electron transfer leads to the generation of holes that are positively charged and reside in VB and electrons in VB. These charge carriers are responsible for the degradation of pollutants [25]. The redox species these charge carriers produce after sunlight irradiation are extremely reactive. These species interact with recalcitrant dyes and degrade pollutants and bacterial cell walls into non-toxic substances [62]. Hence, facile fabrication of such non-toxic metal oxide-based ternary systems as antibacterial agents and sun-light harvesting photocatalysts is inevitable for a clean environment [31]. Among all semiconductor materials, metal oxides and sulphides have been extensively studied owing to excellent catalytic, optical, and electrical properties [3].

Metal tungstates are ternary semiconductor photocatalysts that have been extensively studied because of their photocatalytic ability. The bandgap energies of ternary metal tungstates make them effective and practical visible-light-driven photocatalytic materials. Silver tungstate (A_2WO_4) is a ternary compound of unique tailorable optical and electronic properties. The decomposition of silver tungstate to silver nanoparticles on exposure to visible light makes it highly unstable. This is usually improved by coupling the compound with some other metal oxides or sulphides. Silver-based compounds show a vast spectrum of anti-bacterial activities. These compounds exhibit strong bactericidal effects. Silver ions upon interaction with bacteria attack enzymes and proteins which are responsible for the functioning of bacteria. Therefore, silver is of unique interest as an antimicrobial agent and as a photocatalyst [67,21]. These ternary compounds are non-toxic, easily available, and stable and have been applied for various applications from water and air purification, bacterial disinfection, CO_2 photoreduction, and water splitting [48]. But, the charge transfer property of a single metal oxide photocatalyst is restricted owing to the quick recombination of electrons and holes. This electron/hole recombination leads to less quantum efficiency. This charge carrier recombination is reduced by various methods like heterojunction formation, doping, and dye sensitization [27,7].

Metal dichalcogenides are another unique class of heterogenous semiconductor materials having layered sandwich structures possessing large surface areas making them suitable for coupling with other metal-oxides for enhanced charge transfer [66]. Molybdenum disulphide (MoS_2) is the most widely studied metal dichalcogenide material for wastewater treatment because of its low cost and stability in an aqueous medium. MoS_2 having a narrow bandgap of 1.2 eV, makes it suitable for degradation in both the ultraviolet and visible regions of the solar spectrum [17]. MoS_2 possesses a two-dimensional Multi-layer structure with layers held by van der Waals forces but the fast recombining of charge carriers and lesser conductivity confines its role as co-catalyst. Along with support materials such as Graphene oxide (GO), MoS_2 behaves as an excellent co-catalysts in restricting recombination and stimulating charge transfer at a faster rate [27].

Graphene oxide act as an excellent support material and electron reservoir in ternary heterojunctions by capturing electrons coming from metal oxides [52]. This hindrance in the recombination of charge carriers increases photo-response and increases [14]the stability of hybrid materials for their various applications. The graphene-based composites also show toxicity toward bacteria and have been now extensively used owing to their antimicrobial properties (Ahmad *et al.* 2016). Silver tungstate-based heterogeneous photocatalysts have been effectively employed for photocatalysis and antimicrobial applications. Previously, hybrid silver tungstate-based nanocomposite (La_6WO_{12}/Ag_2WO_4) showed enhanced methylene blue degradation and antibacterial activity for E.coli. Similarly, different other silver tungstates composite such as $Ag_2WO_4/CoWO_4$ [11], Ag_2WO_4/ZnS [22] and Ag_2WO_4/CoS [23] and Ag_2WO_4/CoS [24] showed excellent antimicrobial and photocatalytic activity under sunlight.

The drawback of single ternary or binary compounds is the rapid recombination of charge carriers which hinders their photocatalytic activity. Based on the above remarks and to overcome limitations of individual and binary components, ternary hybrid nanocomposite with carbon-based support structure was prepared in which Ag_2WO_4 is deposited over ultra Thin MoS_2 nanosheets to enhance its surface area, adsorption capacity, stability and to minimize its aggregation and recombination of electron-hole pairs.

The limitations of binary composites can be avoided by combining them with suitable support material. Previous research studies proved that binary combinations of silver-based compounds and metal sulphides are a feasible way to construct photocatalysts with high-performance antimicrobial and photocatalytic activities. But, limited research has been done on the ternary heterojunction formed as a result of metal tungstates and metal sulphides together with carbon-based support materials. In our previous research study, we found that MoS_2 has excellent photocatalytic abilities when it combines with other photocatalysts by exposing more active sites at the interface heterojunction [42,54]. Hence, it has been proved that silver tungstate and sulphides are effective materials both as photocatalysts and antimicrobial agents [24].

Herein, a novel ternary visible light active Ag_2WO_4-MoS_2-GO (AgWMG) nanocomposite was synthesized using a hydrothermal approach. Such ternary silver tungstate-based ternary heterojunction has been prepared and employed for photocatalytic and antimicrobial application for the first time. The nanocomposite was comprehensively studied by employing various characterization techniques comprising FTIR, SEM-EDS, TEM, XRD, XPS, BET, PL, and UV–visible spectroscopy. The photocatalytic activity was evaluated by degradation of anionic dye Methyl orange (MO) under conditions of pH, initial dye concentration, catalyst dose, and irradiation time by ternary AgWMG and binary Silver-tungstate-GO (AgWG) and MoS_2-Graphene oxide (MG). The new ternary composite revealed enhanced photocatalytic activity due to better separation of charge carriers at interfaces of Ag_2WO_6 and MoS_2 in ternary heterojunction. The response surface methodology (RSM) was employed to study the effect among various variables. The antibacterial activity of ternary AgWMG and its binary counterparts was done against Gram-positive (*S.aureus*) and Gram-negative bacteria (*E.coli*). The silver tungstate-based ternary hybrid showed improved photocatalytic and antibacterial properties.

2. Material and methods

2.1. Chemicals

All chemicals and reagents used during the synthesis and experimental procedures were analytical-grade chemicals and were used as such without further purification. Sodium molybdate dihydrate ($Na_2MoO_4{\cdot}2H_2O$, 99 %), sodium hydroxide (NaOH pellets, 98 %), Sodium tungstate dihydrate ($Na_2WO_4{\cdot}2H_2O$), Silver nitrate, ($AgNO_3$, 97 %) sodium nitrate ($NaNO_3$, 98 %), hydrochloric acid (HCl, 35 % w/w), potassium permanganate ($KMnO_4$ >99 %), were purchased from Sigma Aldrich. Isopropyl alcohol (IPA, 99.8 %), (EDTA), was obtained from UNI-CHEM reagents. Thioacetamide (CH_3CSNH_2, 98 %) and Graphite powder (99 % pure for Graphene oxide synthesis) were obtained from Scharlau. Analytical grade (99 % pure) ethylene glycol was acquired from Sigma Aldrich. Ethanol (C_2H_5OH) with 95.6 % purity) was obtained from Merck and dye methyl orange from Fischer scientific company. Distilled water was used for synthesis and reaction procedures.

2.2. Synthesis of ternary silver tungstate-MoS_2-GO (AgWMG) nanoparticles

The ternary AgWMG nanocomposite was prepared by an in-situ two-step hydrothermal method. Initially, Molybdenum disulphide was prepared by dissolving 0.5 mmol of $Na_2MoO_4{\cdot}2H_2O$ and 10 mmol of thioacetamide (CH_3CSNH_2) in 80 ml of distilled water. The whole mixture

was stirred until homogenously mixed and was poured into a 100 ml Teflon-lined hydrothermal autoclave, placed at an elevated temperature of (180 °C) inside the oven for nearly a day. The obtained powder, black in appearance was 3 times washed using distilled water and analytical-grade ethanol. Later, it was dried out at 70 °C in the oven for about 12 h. For the preparation of graphene oxide, the modified Hummers method was used, as explained earlier in our work [54]. Further, $Na_2WO_4{\cdot}2H_2O$ (2.5 mmol, 0.5876 gms) was dissolved in 30 ml distilled water, and Silver nitrate (5 mmol) (0.679 gms) was dissolved in about 30 ml analytical grade ethylene glycol, under continuous magnetic stirring. The sodium tungstate solution was added dropwise in silver nitrate solution for about two hours under vigorous stirring. Meanwhile, the above hydrothermally prepared MoS_2 (0.3 gms) and GO (0.2 gms) were dispersed by ultrasonication for about an hour and added dropwise in the above silver tungstate mixture. The final mixture of the ternary heterogeneous composite was stirred for another hour and was finally poured into a 250 ml Teflon-lined autoclave for hydrothermal treatment at 180 °C for about a day. The obtained shiny greyish black product AgWMG was three times washed with ethanol and distilled water for removal of impurities and was desiccated in the oven at ambient heat. The pictorial description of the hydrothermal synthesis of ternary AgWMG is depicted in Fig. 1.

2.3. Characterization of prepared materials:

The Phase transition studies and crystallization of the ternary photocatalysts were done by the X-ray Diffraction (XRD) (Bruker D8 Advanced equipment) having Cu Ka irradiation and (wavelength = 0.15406 nm) from 2θ values of 10° to 80°. The morphologies, microstructure, and elemental analysis were studied through a Scanning electron microscope (SEM) attached with Energy dispersive X-ray spectroscopy (EDS). Transmission electron microscopy (TEM) was performed to find surface morphology. The surface characterization of the prepared catalyst for revealing the existence of several functional groups was done through Fourier Transform infra-red spectroscopy (FTIR, Thermo Nicolet). The elemental states and chemical composition of the catalyst surface were examined with XPS (Escalab 250- XPS system, Thermo scientific, Uk). A Brunauer–Emmett–Teller (BET) surface analyzer (Nova 2200e Quantachrome) was used for analyzing the surface area and surface porosity. The photoluminescence spectra of the binary and ternary nanocomposites were studied using Shimadzu RF-5301PC, spectro-fluorophotometer, and the excitation wavelength for PL analysis was 325 nm for both samples. The UV-Visible spectra of all the samples were obtained between the range of 300–800 nm on the UV-vis spectrophotometer (Shimadzu, model UV 3600).

2.4. Photocatalytic test

The photocatalytic activity of prepared hybrid ternary and binary composites was assessed by Photocatalytic degradation of anionic dye Methyl orange (MO) under sunlight and Ultraviolet light. The degradation was carried out under ambient conditions in natural sunlight. About 100 ml of dye solutions with an initial dye concentration of 10 ppm and catalyst loading of 50 mg were added to a beaker to perform the degradation experiment. The solution was ultrasonicated to disperse the nanoparticles. The sample suspension was kept in dark for about thirty minutes before placing the solution under sunlight, with continuous stirring to achieve adsorption-desorption equilibrium between the components. The adsorption-desorption equilibrium is essential for achieving maximum adsorption of target pollutants over the surface of photocatalysts. The solution was then placed in sunlight with continuous shaking in an orbital shaking. The absorbance of the solution was checked at regular intervals by taking and separating 10 ml solution through centrifugation at a speed of 6000 rpm. The supernatant liquid was tested for estimating the concentration of MO in solution with the help of a double-beam spectrophotometer at a wavelength of 464 nm. The same experiment was also performed under Ultraviolet light (UV). With each experiment, a blank experiment was also performed without a catalyst which confirmed that no distinct catalytic activity was observed in absence of catalyst/light and under UV light. The degradation performance of catalysts AgWMG, AgWG, and MG were evaluated by the following expression.

$$\%\,\textbf{Degradation} = 1 - \frac{\mathbf{A}}{\mathbf{Ao}} \times 100 \tag{1}$$

Eq. (1) describes the initial absorbance designated by (Ao) and, A is related to absorbance taken once irradiation of solution under sunlight was performed. A solar power meter (SM206) and light meter (HS1010A) were utilized for assessing sunlight intensity and brightness. The photo-stability of the catalyst was checked by reusing the catalyst five times under identical optimized conditions.

2.5. Antibacterial test

The samples were individually tested against Gram-positive bacteria (*Staphylococcus aureus*) and Gram-negative bacteria (*E.coli*) and taken as model micro-organisms using the disc diffusion method. The identity and purity of strains were verified by the Institute of Microbiology,

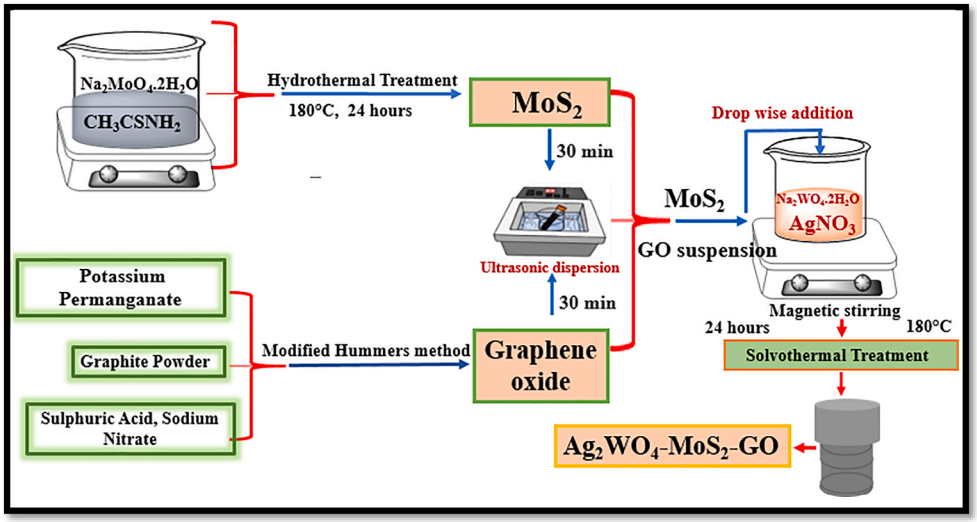

Fig. 1. Illustrative hydrothermal synthesis explanation of ternary AgWMG nanocomposite.

University of Agriculture, Faisalabad, Pakistan. The selected bacterial strains were cultured overnight at 37 °C in (Oxoid, UK) nutrient agar in an incubator. The solution was centrifuged for about 10 min and harvested bacterial colony was washed with phosphate buffer saline. After discarding the supernatant, 100 μL suspension of tested bacteria having 10^7 colony-forming units (CFU)/mL of bacteria cells were streaked on nutrient agar medium after solidification of agar plates. The filtered discs were saturated with a compound solution formerly inoculated with tested microorganisms. Ciprofloxacin (Oxoid, Uk/0 was used as a positive control for bacterial strains for evaluation. Plates after about two hours at 4 °C were precisely incubated at 37 °C for about 20 h. The antimicrobial activity was estimated by measuring growth inhibition zones developed around samples measured in millimeters (mm).

2.6. Response surface methodology (RSM)

RSM is a modern mathematical and statistical combination to optimize the photocatalytic degradation process and evaluate the effectiveness of various interacting parameters. This approach provides reliable results while predicting the response of various variables simultaneously. In the present research study, the central composite design (CCD) of RSM was designated for cumulative response and, adequacy assessment of the model.

3. Characterization

3.1. FTIR analysis

The presence of numerous functional groups and the formation of chemical bonds in ternary silver-tungstate-based nanocomposites shown in Fig. 2. were evaluated using Fourier transform infrared (FTIR) analysis. Transmittance peaks are observed at 650 cm^{-1}, 845 cm^{-1}, 986 cm^{-1}, 1385 cm^{-1}, and 1045 cm^{-1}. In the ternary AgWMG, elongated broadband is present at 650 cm^{-1} which is accredited to the W-O bond stretching vibrations which are characteristics of WO_4^{-2} species in all tungstates [55]. The small transmittance peak existing at 1385 cm^{-1} is assigned to Mo-O and S—O—S vibrations of MoS_2 and is typically absent in binary AgWG nanocomposite. [43]. The peak present at 1385 cm^{-1} shows stretching vibrations caused due to typical O-W-O bonds inside distorted clusters in ternary heterojunctions [39]. Similarly, in all samples, the peak present at 1045 cm^{-1} and the presence of skeletal vibrations are due to the carbonyl linkage confirming the presence of graphene oxide in all the composites [37]. Due to the less content of graphene oxide in the composites, no additional transmittance peaks were observed [28].

3.2. XRD analysis

The technique of X-ray diffraction is used to investigate crystallinity, d-spacing between planes, and the average grain size of pristine, binary, and ternary nanoparticles (Fig. 3). The distinctive peaks of silver tungstate obtained are present at 2θ values of 10.98°, 16.71°, 30.27°, 31.63°, 33.09°, 34.43°, 45.45°, 54.66°, 55.42°, 57.19°, 58.16°, 66.07°, 75.27° indexed at crystal planes (1 1 0), (0 1 1), (0 0 2), (2 3 1), (4 0 0), (4 0 2), (3 6 1), (0 6 2), (4 6 0), (3 3 3), (2 1 4), and (6 3 3) respectively (JCPDS card No.28–1023). All these peaks correspond to Ag_2WO_4 (α-phase) [55]. The distinctive (0 0 2) peak of silver tungstate can be seen in all composites confirming the formation of silver tungstate. The main peaks of MoS_2 are being observed at 14.69°, 31.49°, 36.03°, 43.6°, and 57.78° at corresponding crystal planes of (0 0 2), (1 0 0), (1 0 2), (0 0 6), and (1 1 0) JCPDS card (No. 37–1492). The key peak at $2\theta = 14.69°$ can be observed only in the ternary sample indexed to the (0 0 2) plane confirming the successful synthesis of MoS_2 in the ternary hybrid. The basal (0 0 2) plane of MoS_2 implies developed stacking layers along the c-axis and lamellar structure. Moreover, the d-spacing of the (0 0 2) plane calculated as 0.623 nm suggests the presence of a hexagonal phase of MoS_2 [5]. All the diffraction planes match very well with studies done previously [65]. A prominent peak at $2\theta = 13.6°$ with a d-spacing of 0.38 nm in the XRD pattern of ternary AgWMG nanocomposite, credited to (0 0 1) plane of graphene oxide confirming its synthesis. The binary silver-tungstate/GO (AgWG) **(3c)** clearly shows this peak confirming the formation of GO in binary and ternary hybrids which is absent in pristine silver tungstate (AgW) **(3b)**. The sharp peaks appearing at $2\theta = 26.7°$ in ternary AgWMG, corresponding to the plane (0 0 2) might be accredited to restacked graphene sheets in short-range order [1]. This plane suggests graphitic planes of GO with minimal oxygen functional groups labeled as reduced graphene oxide [45]. The sharp GO peak in ternary hybrid as compared to binary suggests that the ordered structure of GO may have been intercepted by interaction with silver tungstate and MoS_2 and silver particles had intercalated GO layers leading to non-uniformity of stacking. The absence of any other impurity peak suggests structural integrity, fine crystalline nature, and high phase purity of prepared nanocomposites. It can be seen that the peaks in ternary nanocomposite are intense and more prominent suggesting the successful coupling of silver tungstate lattice with MoS_2 and insertion of GO support [43].

$$D = K\lambda/\beta\cos\theta \quad (2)$$

Here, D is the crystalline size of the nanoparticle, λ is X-ray wavelength (0.154 nm), β is related to FWHM (full width at half maximum) of catalysts, and K is the Scherrer constant with the value of 0.94, and the diffraction angle is (θ). The crystallite sizes calculated from the sheerer

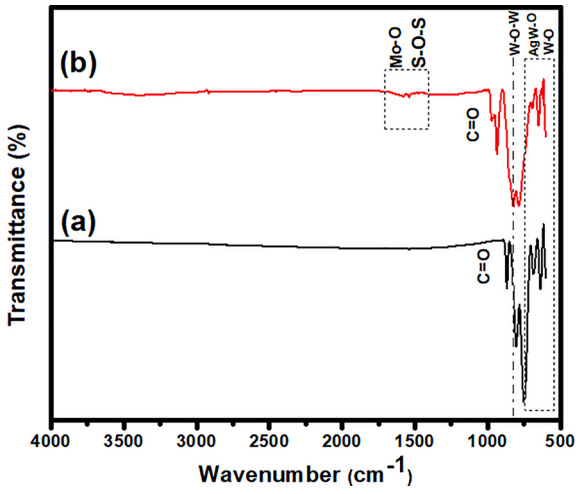

Fig. 2. FTIR spectra (a) binary AgWG (b) ternary AgWMG.

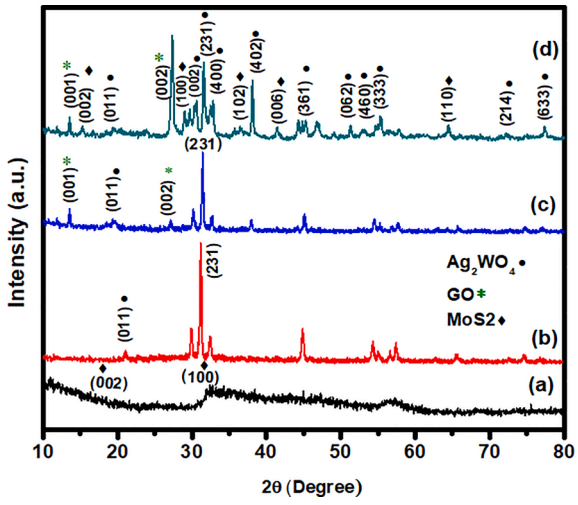

Fig. 3. X-ray diffraction analysis (a) MG (b) AgW (c)AgWG (d) AgWMG.

equation for MG, AgWG, and AgWMG, are found to be 27.8 nm 22.5 nm, and 18.65 nm, respectively. The small crystallite size of ternary AgWMG is accredited to fast crystal nucleation and, subsequent growth during the synthesis process. The small size may be due to the lesser dimensions of layered Graphene oxide and MoS_2 [49].

3.3. SEM-EDS analysis

The microstructures and morphology of silver tungstate-based binary and ternary hybrids were examined through SEM images at various resolutions in Fig. 4. The binary Silver tungstate-graphene oxide-based composite Fig. 4(b) show silver tungstate nanorods distributed over graphene oxide sheets. The ternary heterojunction formed after the addition of MoS_2 synthesized through a hydrothermal route shows the Ag_2WO_4crystallizing in form of more uniform nanorods forming a continuous network with flower-like clusters of MoS_2 with relatively sharp edges and uniform lateral size **(4c & d).** Usually, products obtained with hydrothermal synthesis are highly crystalline, selective, pure, and of desired morphology. Moreover, for the formation of ultra-thin sheets of MoS_2 and flower morphology, an elevated temperature is required to minimize agglomeration with other components. Further, this elevated temperature also controls the morphology of individual components in the ternary heterostructure. In ternary nanocomposite, hydrothermally synthesized MoS_2 is an ultra-thin nanosheet structure with high crystallinity as confirmed by previous studies [55]. Coupling of Silver tungstate with MoS_2 and GO support has induced uniformity and crystallinity in the morphology of silver tungstate nanorods. These nanorods are seen growing uniformly from the surface cavities [57]. Bare interlamellar flowers similar to pristine MoS_2 as in (Fig. 4a) can be seen growing and spreading over the broken bunches of tungstate rods [30]. The chances of MoS_2 nanosheet formation in hybrid are quite high at neutral pH, because of availability of molybdenum source in both (MoO_4 and polymolybdate) forms. This sheet structure gives better adsorption and reaction site to composite [55]. The SEM images show the successful synthesis of a ternary hybrid with the presence of all pristine composites. The EDS analysis of ternary AgWMG as shown in Fig. 4(e) shows the complete elemental composition of ternary hybrid with an inset table showing the weight percentages of each element

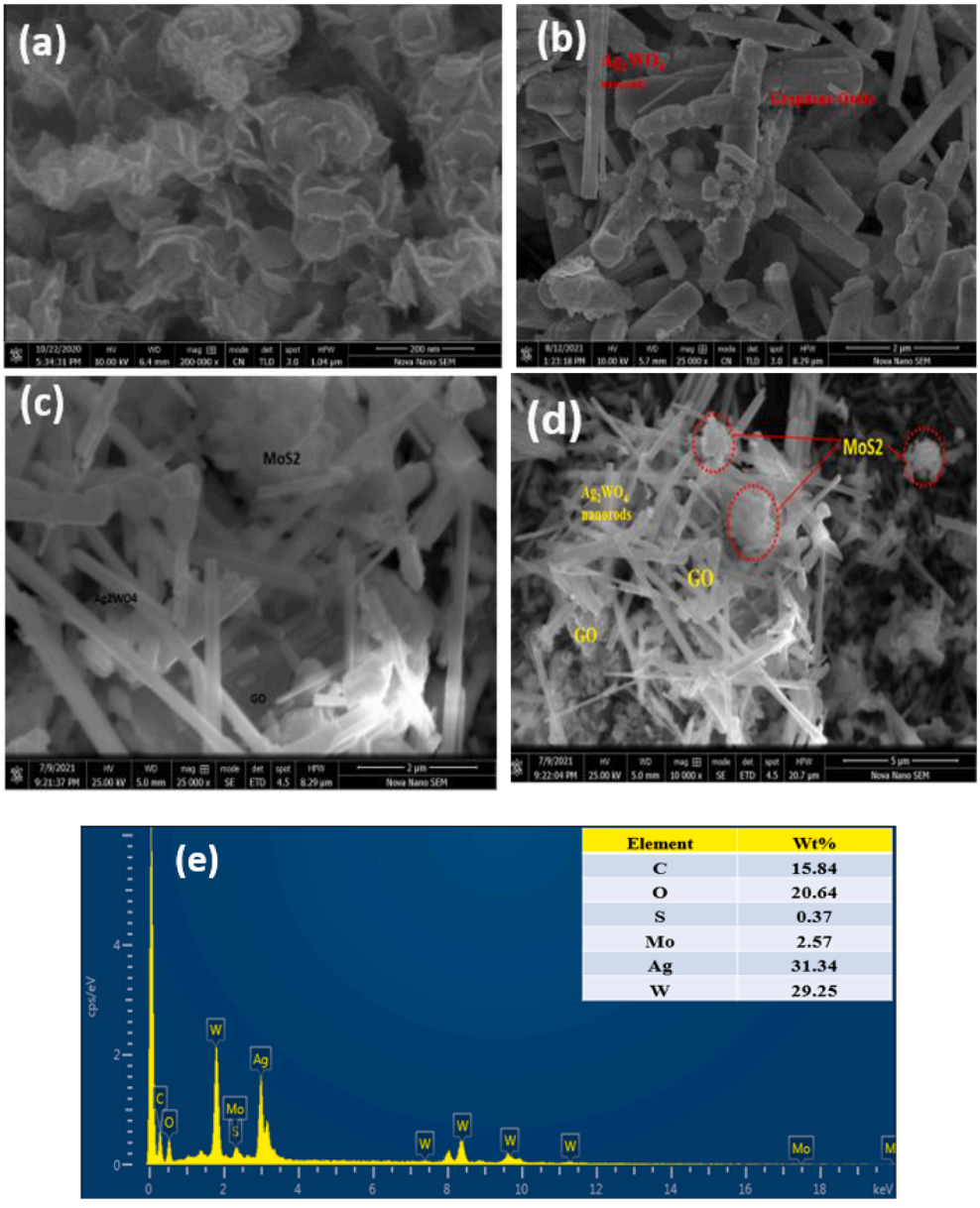

Fig. 4. Scanning electron microscope analysis of (a) MoS_2 (b) AgWG (c, d) AgWMG (e) EDS of AgWMG.

present. Predominantly, peaks of Silver (Ag), Tungsten (W), Sulphur (S), Molybdenum (Mo), Oxygen (O), and Carbon (C) can be seen corresponding to their respective energy levels. The sample contains 31.34 % Ag, 20.64 % O, 29.25 % W, 2.57 % Mo, and 0.37 % Sulphur in the ternary composite. The SEM-EDS results reveal an effective synthesis of ternary AgWMG with no other trace elements. The EDS spectra confirm the homogenous distribution of elements in the ternary hybrid [41].

3.4. TEM analysis

The morphology of the fabricated ternary nanocomposite was further confirmed using TEM and High-resolution transmission electron microscopy (HR-TEM). The ternary hybrid clearly shows nanorod-like structures of silver tungstate with polydispersed and ultra-thin spherical MoS_2 nanosheets randomly distributed over the graphene oxide sheet Fig. 5(a and b). The formation of heterojunction was confirmed by lattice-spacing of 0.623 nm of (002) facet of MoS_2, endorsing the presence of hexagonal phase and (002) facet of silver tungstate (Fig. 5c) indicating the successful formation of ternary nanocomposites. The Ag_2WO_4 nanorods and MoS_2 sheets could be found attached to the Graphene oxide sheet with great uniformity. The homogenous arrangement and uniformity in size of silver tungstate nanorods are due to the synergy of three components. The HR-TEM images revealed the creation of smooth Ag_2WO_4 and MoS_2 heterojunction interfaces in a ternary composite. The SAED patterns show distinct ring formations conforming to the poly-crystalline nature of Ag_2WO_4 and MoS_2 present in the ternary hybrid. The ring patterns matching well with the XRD data point to the formation of a highly crystallized nanocomposite (Fig. 5d) [24].

3.5. XPS analysis

The chemical composition of the fabricated nanocomposite is determined by X-ray photoelectron spectroscopic (XPS) analysis. The XPS spectra of ternary AgWMG show peaks of elements Silver (Ag), Oxygen (O), carbon (C), and Sulphur (S) (Fig. 6a). The elemental composition via XPS survey scan of silver tungstate-based prepared nanocomposites, when examined completely, revealed peaks at W (37.51 eV), O1s (530.2 eV), C1s (284.07 eV), (710.8 eV), and Ag3d (368.3 eV), and Mo3d. The C1s peak is prominently indexed at about 285.2 eV. The $W4f_{7/2}$ and W $4f_{5/2}$ peak, ascribed to the WO_4^{2-} present at binding energy 35.45 eV and 37 eV respectively in the W4f spectrum of Ag_2WO_4. The $3d_{3/2}$ and $Ag3d_{5/2}$ characteristic peaks of Ag 3d spectra are shown at 372.1 eV and 368.3 eV. The atomic percentage is shown in Fig. 6(b). contains Ag3p3, Ag3d, C1s, O1s, W4f, S2p, and Mo3d, is 10.1 %, 17.8 %, 22.9 %, 40.5 %, 6.8 %, 0.9 %, and 1.1 % in AgWMG.

3.6. BET analysis

The most critical parameter to determine the photocatalytic activity of any nanocomposite is its surface area. The surface area is a crucial defining factor for determining the photodegradation efficiency of ternary photocatalysts. The BET adsorption/desorption isotherm of ternary AgWMG and AgWG is shown in Fig. S1. The results show that the ternary nanocomposite follows a type IV isotherm with a hysteresis loop. These types of isotherms are characteristics of mesoporous materials with lamellar structures. The BET (Brunauer-Emmett-Teller) method was used to measure the specific surface area from the adsorption data of nitrogen gas and is found to be 8.630 m^2/g for AgWG, and the specific surface area of AgWMG is 11.134 m^2/g. Table 1, shows a comparison of surface area and pore volume. The higher surface area of the ternary nanocomposite confirms its synthesis. The large surface area was found

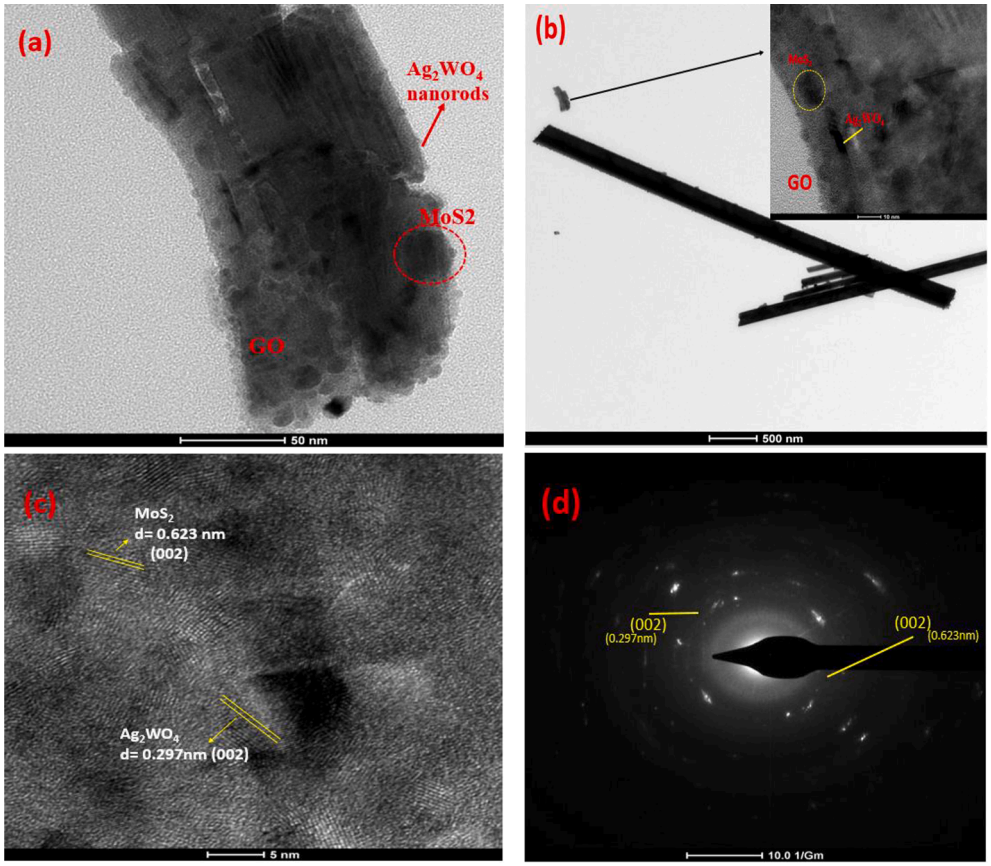

Fig. 5. TEM image of (a and b) AgWMG (c) HR-TEM lattice fringes showing d-spacing of AgWMG (d) SAED pattern of AgWMG.

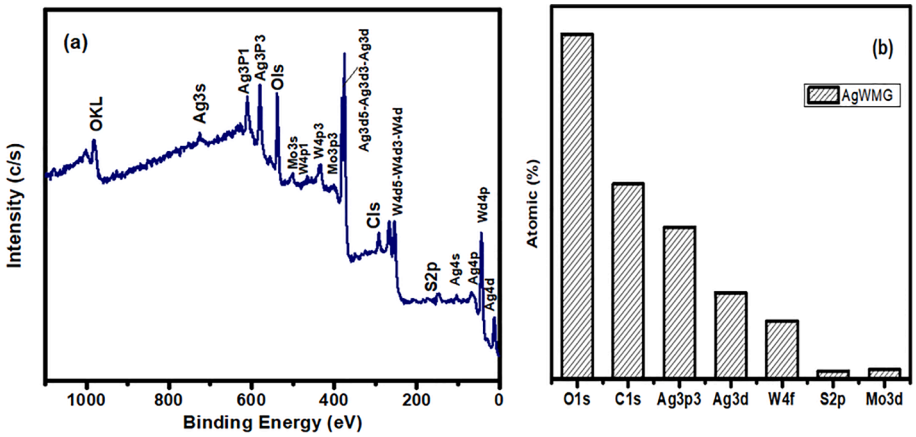

Fig. 6. XPS of (a) AgWMG (b) Atomic percentage of various elements in AgWMG.

Table 1
Summary of Surface area, pore volume, and pore diameter of AgWG and AgWMG nanoparticles.

Photocatalysts	Surface area (m^2/g)	Pore volume (cm^3/g)	Pore diameter (nm)
AgWG	8.630	0.031	12.687 nm
AgWMG	11.134	0.049	14.225 nm

after coupling of silver tungstate and resultant heterojunction formation with MoS_2. The enhanced surface area confirms that more molecules of pollutants are adsorbed on the surface of the catalyst and more active radicals are produced. This also increases the availability of more light absorption directly increasing photocatalyst efficiency [63].

3.7. Photoluminescence analysis

The separation of light-induced charge carriers, their transfer from various interfaces, and recombination is best understood using the Photoluminescence technique. Fig. 7. shows PL spectra comparison of binary and ternary nanocomposite for e-/h + pairs separation efficiency. The results suggest that the weaker the PL intensity, the higher the charge separation efficiency of the nanocomposite [12]. The more intense peak of binary AgWG suggests that more emissions occur as a result of a higher rate of recombination of photo-generated charge carriers.

A decline in photoemission and peak intensity in the ternary sample confirmed the suppression of recombination of electrons and holes, consequently leading to an enhancement in photocatalytic activity. This interaction among ternary heterojunctions may also lead to the development of some surface defects, that might provide active sites for the attachment of pollutants. Hence, as compared with the binary composite, the ternary AgWMG exhibited higher photocatalytic degradation efficiency due to suppression in charge carriers recombination [32].

3.8. Optical properties

For efficient photodegradation processes, a range of the optimum requirement of light is crucial for optical properties and bandgap determination of various photocatalysts (Fig. 8). The Energy bandgaps of synthesized binary and ternary nanocomposites were estimated by tauc plot [51]. The optical absorption of prepared samples was studied in the UV–vis range from 300 to 800 nm. The formula used for the calculation of bandgap by tauc plot is given below.

Hence, it is consistent with the results of XRD, XPS, and FTIR proving successful synthesis of the ternary nanocomposite. Moreover, it was confirmed from the bandgap that ternary AgWMG showed high degradation in visible light due to the effective separation of electron-hole pairs [52].

$$(\alpha h\nu)^2 = B(h\nu - Eg) \quad (3)$$

In this equation, Eg = hν, after (αhν is 0) and, then $(\alpha h\nu)^2$ versus energy (eV)is plotted. The absorption energy is determined at (hν) value

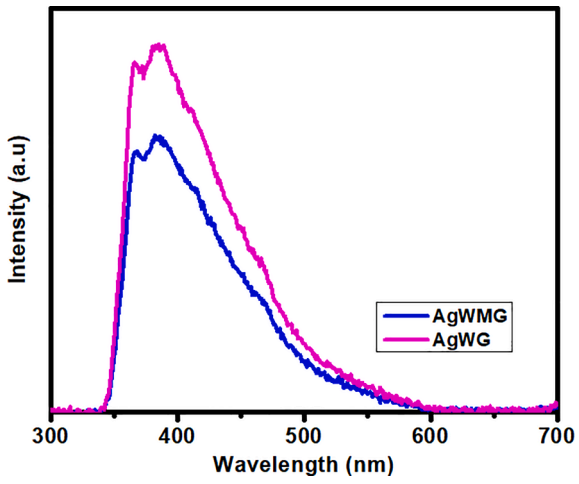

Fig. 7. Photoluminescence spectra of binary AgWG and ternary AgWMG.

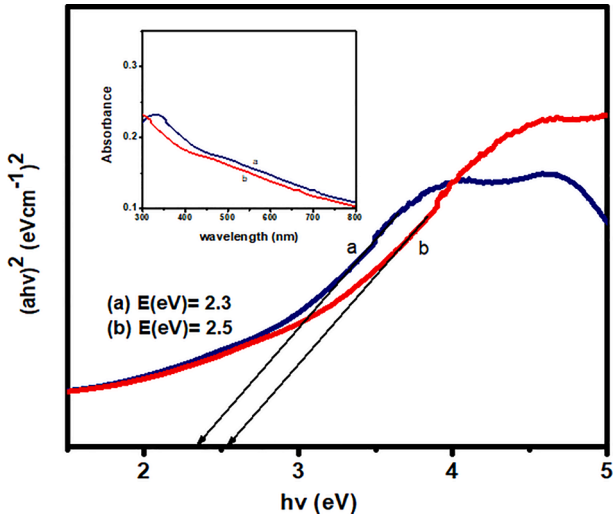

Fig. 8. UV-vis Tauc plot bandgap of (a) AgWMG (b) AgWG.

and extrapolated to α = 0. The estimated bandgap energies were 2.35 eV, and 2.5 eV for AgWMG and AgWG. In the equation, parameters (α, B, and ν) denote the absorption coefficient, proportionality constant, and light frequency. The bandgap values suggest that catalysts are active in visible light regions of the solar spectrum [16],

4. Effect of various working parameters on methyl orange degradation

4.1. Effect of pH

The most adjustable working parameter for photocatalytic dye degradation is the pH of the aqueous solution as it can affect reaction rates in several ways. The surface charge properties of the catalyst are dependent on pH. Hence, pH directly affects dye adsorption on catalyst surfaces depending on the nature of functional groups on the surface. At a particular pH, the surface charge of the catalyst is modified to a particular charge which favors dye molecule adsorption [43]. The experiment was performed under sunlight by changing the pH of the dye solution from 2 to 9 by keeping the catalysts dose fixed at 50 mg/100 ml for AgWMG and 70 mg/100 ml for binary catalysts, 10 ppm of MO initial concentration, and, radiation period of 90 min for all three catalysts. The results of experiments are presented in Fig. 9(a), which reveals that at pH 5 degradation rate is very high above 90 %, which remained almost unchanged till pH 7 and then started decreasing as pH increased. The MO degradation ratio decreased with the subsequent increase in pH in presence of catalyst AgWMG, indicating that acidic conditions remained more favorable for the degradation of MO by ternary AgWMG under sunlight. The acid-base properties of semiconductor metal-oxide-based composites significantly affect the photocatalytic property of the composites. The adsorbent surface gets positively charged at a pH value less than the pH_{PZC} value where it behaves as cation-repelling and anion-attracting [38]. In contrast, the surface is negatively charged above the pH_{PZC} value and attracts cations, and resists anions. The point of zero charges (pH_{PZC}) of AgWMG as calculated by the pH drift method was 6.2. [40]. The electrostatic repulsion between AgWMG surface and methyl orange increases with increased pH, obstructing MO to close the AgWMG surface and decrease MO degradation. The catalyst surface becomes negatively charged and positively charged at pH above and below this pH_{PZC} [50]. Methyl orange is an anionic dye that is negatively charged upon dissociation in an aqueous solution. Initially at a pH value of 2, when MO molecules started getting protonated degradation rate was quite low. Upon increasing the pH from 4 to 6, negatively charged MO molecules were attracted to positively charged surface of AgWMG leading to an increase in degradation rate. Hence, at pH < pHpzc the ternary nanocomposite exhibited excellent photocatalytic activity. But at a higher value (pH > pHpzc), the negatively charged surface of the catalyst resisted the adsorption of anionic MO molecules and hence a prominent decrease in MO degradation was observed [36]. Binary AgWG and MG at pH 6 and 7 respectively showed 87 % and 85 % degradation in sunlight.

4.2. Influence of catalyst dose

The pollutant degradation is affected by the amount of catalyst utilized during experiments as shown in (Fig. 9b) The optimization of the catalyst is very important for assessing the economic feasibility of the reaction and effectiveness of the catalyst [44]. Usually, by increasing the photocatalyst amount, photodegradation also increases. This is ascribed to an increased number of active catalyst sites on its surface as the amount is increased. This leads to hydroxyl radical and superoxide radicals production which is responsible for dye degradation [47]. The

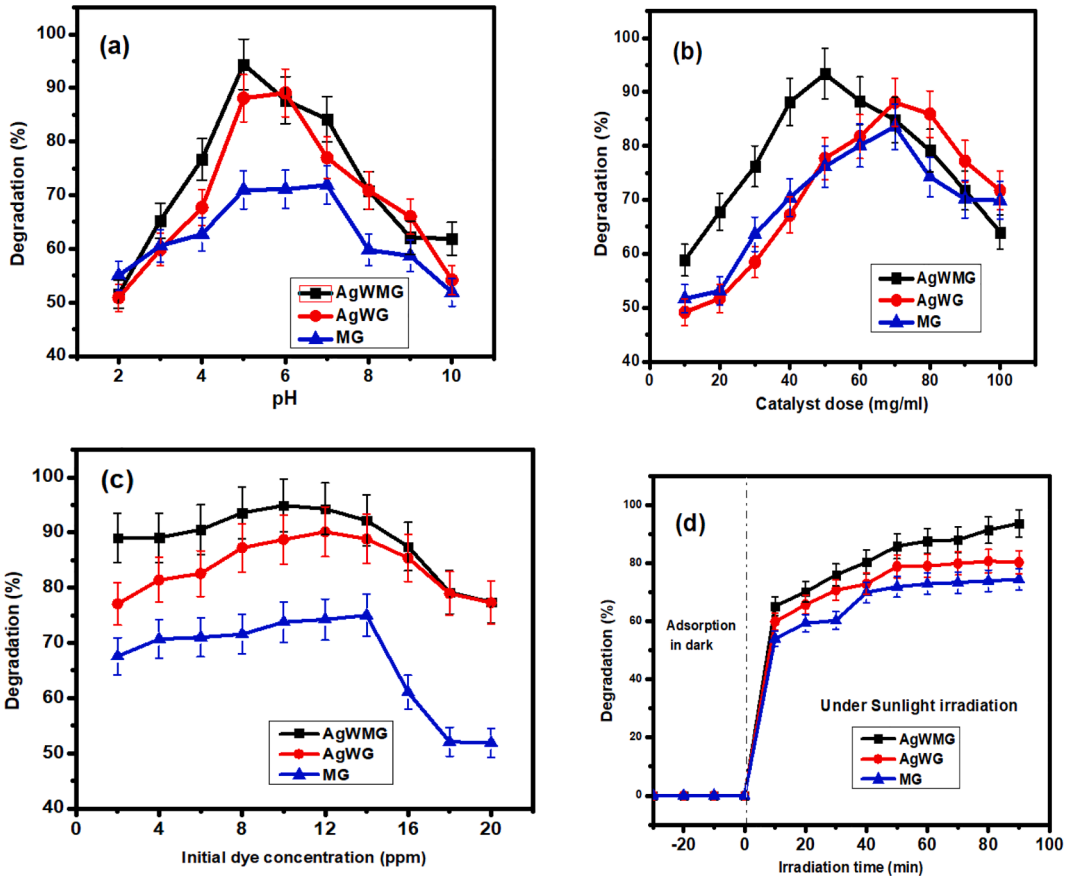

Fig. 9. optimization of (a) Solution pH (b) nanocomposite loading (c) IDC (d) Contact time for MO degradation in sunlight radiation.

effect was explored by changing the concentration of catalyst loading from 10 mg/100 ml of dye solution to 100 mg/100 ml for binary and ternary catalysts. Initially, degradation increased upon the increase and reached a maximum at the value of 50 mg/100 ml. But, above this optimal value, the degradation rate of MO started decreasing. The photoactive volume was decreased due to turbidity and agglomeration of AgWMG particles. This ultimately restricted the penetration of sunlight irradiation on the catalyst surface and decreased the dye degradation [26]. The higher degradation was credited to silver nanoparticles in the silver tungstate-based ternary nanocomposite.

4.3. Influence of initial MO concentration

The optimization of initial dye concentration (IDC) provides information regarding the driving force for overcoming mass transfer resistance between catalyst and dye solution and the adsorption of dye molecules on catalyst active sites (Fig. 9c) [10]. The dye degradation was initially increased with the increase in dye concentration from 2 ppm to 10 ppm, after which it started decreasing. This is ascribed to the coverage of a relative portion of catalyst-active sites by dye molecules and a decline in the production of reactive hydroxyl radicals [56]. Moreover, the light dyed-screening i.e the phenomena of mutual screens between MO molecules and AgWMG surface due to increased concentration of dye hinders light absorption and transmission. The results state that effective degradation is achieved with lower concentrations of dye being used [20].

4.4. Influence of contact time

The influence of time of light exposure on MO removal by ternary AgWMG is shown in Fig. 9(d). The results displayed a linear relationship between time and percent degradation signifying that degradation was enhanced with a subsequent increase in light irradiation. This was because eventually as a result of increased irradiation time, an increased reaction rate occurred leading to better production of electron-hole pairs. This finally increases the chances of interaction between the dye molecule and e^-/h^+ pairs [13]. Studies have shown that degradation increased from 40 % to 93 % as time increased from 20 to 90 min. The improved degradation efficiency of catalysts is ascribed to the fact that their photocatalytic activity increases overextending irradiation time, exposing pollutant molecules to more free radicals for more time duration [53].

4.5. Kinetics of photodegradation reaction

For the photodegradation of methyl orange by ternary AgWMG and binary AgWG and MG nanocomposites, first-order and second-order kinetic models were examined. Photocatalytic degradation of organic pollutants by metal tungstate-based composites usually follows first-order kinetics [14]. The equations of each model are represented in Eqs. (3) and (4).

First-order kinetics:

$$\ln\frac{Co}{Ct} = k_1 t \tag{4}$$

Second-order kinetics:

$$\frac{1}{Ct} - \frac{1}{\mathrm{Co}} = \mathrm{k_2 t} \tag{5}$$

Relationship between ln(Co/Ct) and, time of irradiation, illustrates a straight line where Co and Ct signify original and final concentrations, shown in Fig. 10. The results state that MO photo-degradation by ternary AgWMG nanocomposite follows well first-order kinetics. A straight line appears when Co/Ct is drawn against time and, the linear regression slope gets equal to (k) i.e. apparent rate constant of first-order. The higher rate constants k of ternary composite indicates that AgWMG is more efficient under sunlight than its counterparts counterpart. The values of R^2 for the first-order reaction ternaryAgWMG, binary AgWG, and MG are 0.9876, 0.9976, and 0.9727, proposing that all these hybrids successfully follow the first-order reaction (Table.2).

4.6. Reusability

The practical applications and economical feasibility of catalysts are determined by the stability and reusability of nanocomposites. Therefore, the recycling of ternary AgWMG catalyst was studied for successive five runs under the optimized conditions of pH = 5, C.Dose = 50 mg/100 ml, IDC = 10 ppm, and time duration of one and a half hours. After an individual run, the catalyst was recovered from the treated MO solution, it was washed, dried at 60 °C, and reused. After each cycle, there was an insignificant reduction in MO degradation. The synthesized ternary Photocatalyst shows outstanding high efficiency under sunlight for MO degradation whose results are summarized in Fig. 11. The synergy of three components and the layered structure of co-catalyst and support material provides appropriate characteristics of easy preparation, reusability, and effective removal of pollutants under sunlight.

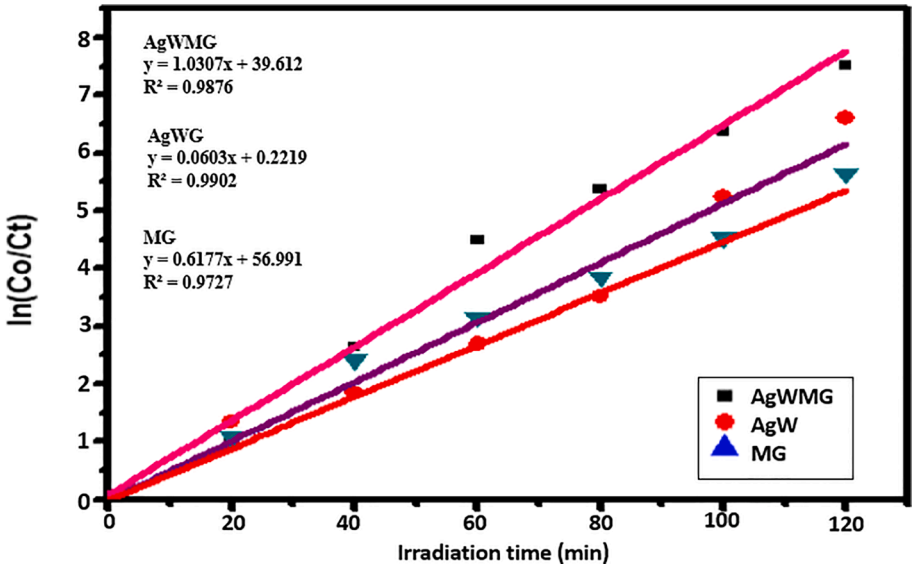

Fig. 10. First-order kinetics model for photocatalytic degradation of MO by AgWMG, AgWG, and MG.

Table 2
Kinectic First order and second order fitting for MO degradation by ternary AgWMG.

Samples	Optimized Experimental conditions			First-order kinetics		Second-order kinetics	
	pH	Photocatalyst dose(mg/100 ml)	IDC (ppm)	k1(min^1)	R^2	K2 ($L\mu mol^1 min^1$)	R^2
AgWMG	5	50 mg	10 ppm	0.08	0.9876	0.421526	0.8357
AgWG	6	70 mg	10 ppm	0.06	0.9902	0.245525	0.7167
MG	7	70 mg	10 ppm	0.6	0.9727	0.147892	0.8287

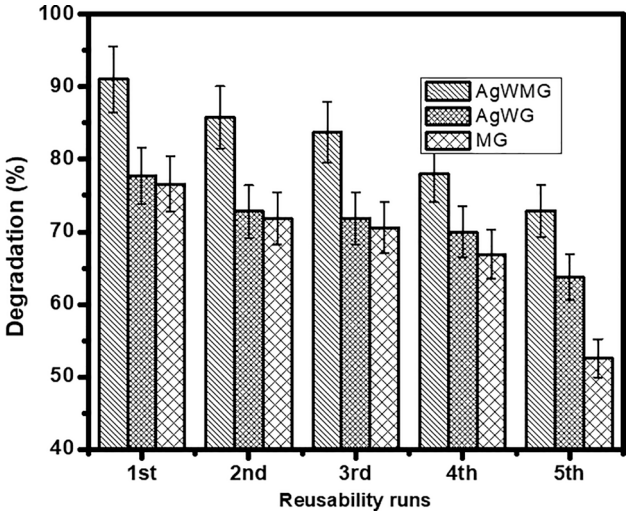

Fig. 11. Reusability study by ternary and binary nanocomposites.

(Table 3 supplementary information) presents a comparison of silver tungstate- and GO-based catalysts for dye degradation and antimicrobial activities.

5. Optimization of nanocomposites using response surface methodology

Response Surface Methodology (RSM) is considered a very common technique among various experimental designs. It is comprised of a set of mathematical and statistical models for optimizing various parameters. The optimization of various parameters for the Photodegradation of Methyl orange was done using a central composite design (CCD). The CCD model is significant for its high predictability of responses and determination of relationships amongst diverse independent variables and responses.

According to the results of batch experiments performed, three operative parameters for MO removal by AgWMG and their probable interactions were studied using the CCD model of RSM. The interactions between time, pH, and catalyst dose were determined using CCD. Design expert-7 which is a statistical software was utilized for optimization and a total of 20 random runs were obtained for maximizing MO degradation under sunlight radiation. The possible effect of all 3 independent variables on dye degradation was analyzed using analysis of variance (ANOVA). The response variable. The percent degradation, which is referred to as the response variable was fitted against experimental variables, using a quadratic model for co-relation. The interaction of 3 variables was explained using a second-order polynomial equation represented.

$$Y = \beta_0 + \beta_1 X_1 + \_\beta_2 X_2 + \beta_3 X_3 + \beta_4 X_4 + \beta_{12} X_1 X_2 + \beta_{13} X_1 X_3 + \beta_{14} X_1 X_4 + \beta_{11} X_1^2 + \beta_{22} X_2^2 + \beta_{33} X_3^2 + \beta_{44} X_4^2 \text{ Eq 6.}$$

The final quadratic equation in terms of coded values is given in **Eq. 7**.

$$\text{MO Degradation (\%)} = +95.18 + 6.00*A + 1.07*B + 8.75*C + 0.000*A*B - 17.50*A*C - 3.25*B*C - 13.35*A^2 - 8.22*B^2 - 7.69*C^2 \text{ Eq. 7.}$$

Here, in terms of coded values, Y denotes the dependent variable while independent variables are factors (A, B, and C). The percentage dye degradation MO is shown by Y and the terms A, B, and C represents pH, catalyst dose (mg/100 ml), and time in minutes respectively. The obtained correlation coefficients (R_2 = 0.9696 and adjusted R_2 = 0.9422) values demonstrated a close fit between experimental and predicted values. This equation can be used to determine the response of every variable at the applied level. Moreover, variables having a positive coefficient value give a high positive effect on response [33].

The value of correlation coefficient (R_2) was 0.9678 revealing 96.7 % of the whole variation for decolorization efficacy as described by the above model. Since most of the p-values were<0.0001, ANOVA for degradation of MO suggested that both model and model terms were significant and the particular quadratic model can expect the degradation efficacy [64]. From ANOVA analysis, the lack of fit is not significant. From Table 4, the obtained F values for pH, contact time, and, catalyst dose are 20.02, 42.57, and 0.63 respectively, showing that pH proved to be the most significant parameter followed by contact time and then catalyst loading.

5.1. Optimization of parameters for MO degradation by ternary AgWMG nanocomposite

The three-dimensional response surface contours were plotted to explain the interaction between two parameters influencing the degradation of dye. Considering this approach, within the experimental ranges two parameters were changed keeping the third parameter constant. To attain the optimized conditions for dye degradation, the upper and lower limits were adjusted to obtain a maximum response. The response surface plots as a function of two variables keeping the third variable constant are shown in Fig. 12. The results clearly showed interactions among all three stated parameters were important.

The studies revealed that the solution pH has the greatest impact on the MO degradation by Ternary AgWMG followed by catalyst dose and time. The results of the interaction among pH and catalyst dose in Fig. 12 (a) contour diagram evidenced that MO degradation was enhanced by enhancing photocatalyst weight and pH, keeping time constant. The variations in surface charge of photocatalyst as pH increased from 2 till 5 and catalyst dose up to form 10 mg/100 ml to 50 mg/100 ml, degradation ability increased due to variations in photocatalysts surface charge and improved attainability of larger number of active sites due to photocatalysts enhanced surface area [34]. Under optimized conditions, the MO degradation efficiency is 92.8 % and 91.2 % for predicted and experimental values confirming that the designed CCD model for evaluation was precise and reliable [35]. Moreover, the p-values(<0.0001) from the ANOVA table show that the interaction effect between catalyst dose and dye solution pH was significant. An increase in both pH and catalyst (AgWMG) dose shows a decrease in degradation efficiency. [4].

The 3-D surface plot of photodegradation of MO shows the removal of pollutants at various values of pH and contact time, keeping the catalyst loading constant at 50 mg/10 ml. The elliptical shape of the contour plot suggested maximum degradation of MO at optimized pH of 5 was achieved as the time of irradiation was increased. The effect is more evident in Fig. 12(b) With reaction conditions of pH (5–6) and contact time of 80–90 min, a removal percentage of (92 %) was precisely acquired.

The interaction effect of time and catalyst dose is revealed in Fig. 12

Table 4
ANOVA Table for MO degradation optimization by ternary AgWMG.

Source	Sum of squares	df	Mean square	F Value	p-value Prob > F	
Model	7829.59	9	869.95	35.42	*< 0.0001	significant
A-pH	491.80	1	491.80	20.02	0.0012	
B-catalyst dose	15.49	1	15.49	0.63	0.4455	
C-time	1045.63	1	1045.63	42.57	*< 0.0001	
AB	0.000	1	0.000	0.000	*<0.0001	
AC	2450.00	1	2450.00	99.75	*< 0.0001	
BC	84.50	1	84.50	3.44	0.0933	
A^2	2566.76	1	2566.76	104.51	*< 0.0001	
B^2	973.55	1	973.55	39.64	*< 0.0001	
C^2	851.97	1	851.97	34.69	0.0002	
Residual	245.61	10	24.56			
Lack of Fit	245.61	5	49.12	3.21	0.0528	Non-significant
Pure Error	46.1	5	6.1			
Cor Total	8075.20	19				
Std. Dev.	4.96		R-Squared			0.9696
Mean	75.20		Adj R-Squared			0.9422
C.V. %	6.59		Pred R-Squared			0.7648
PRESS	1899.65		Adeq Precision			18.782

*Significant model terms in ANOVA.

(c) of the response surface diagram revealing positive effects on MO degradation. The figure shows that degradation efficacy increased by enhancing both parameters which means both parameters showed good interaction effects for the removal of dye pollutants. This can be proved by the ANOVA table indicating a significant coefficient of interaction between these two factors (P = 0.0933). High.

High proficiency of individual parameters could be a reason for insignificant interactions among these parameters, making the effect of these parameters' interactions insignificant [13].

6. Photocatalytic degradation mechanism by ternary AgWMG nanocomposite under sunlight

Earlier research works have revealed that the degradation of dyes is because of the formation of reactive species such as photoinduced hydroxyl radicals, electrons, holes, and superoxide anion. The active radicals including electrons, holes, superoxide radicals, and hydroxyl radicals were scavenged by appropriate scavengers to investigate the scavengers playing a crucial role in the degradation of MO by ternary AgWMG under sunlight. Under the following experimental conditions (pH = 5, catalyst loading = 50 mg/100 ml, IDC = 10 ppm, and 90 min for continuous shaking under sunlight), firstly EDTA, potassium dichromate ($K_2Cr_2O_7$), followed by DMSO, and ascorbic acid were used as scavenging agents against holes, electrons, hydroxyl, and, superoxide ($O_2^{-2)}$) radicals. The experiment was performed under sunlight and the concentration of each scavenger was kept 5 Mm. Fig. 13 shows the effect of the addition of numerous scavengers on MO degradation using AgWMG photocatalyst. Upon addition of EDTA and DMSO, the results specify, that maximum lessening in photocatalytic activity was detected and, then by ascorbic acid and the least by $K_2Cr_2O_7$. The EDTA addition reduced photocatalytic activity from 97 % to 48.85 % and DMSO and ascorbic acid decreased degradation from 93 % to 51 % and 69 % respectively. The trend confirmed that photogenerated h^+, hydroxyl radicals, and superoxide radicals played a major role while electrons were the minor reactive species in the MO degradation.

The proposed mechanism pathways for the MO photodegradation by the ternary photocatalyst is as follows shown in Fig. 14.

Under sunlight irradiation, both silver tungstate and MoS_2 were excited, leading to the generation of e^-/h^+ and holes in their conduction bands (CB) and valence bands (VB) respectively. When the AgWMG heterojunction was irradiated by photons possessing energy greater than their bandgap, the electrons in the VBs of MoS_2 and silver tungstate are excited from the VBs to the CBs, leaving holes on VB. The electrons combine with the O_2 present in the solution generating superoxide radical anion while the holes combine with water to produce strong oxidizing agents (hydroxyl radicals), responsible for the degradation. The two semiconductors being in close contact had suitable bandgap widths. The electrons of the Ag_2WO_4 conduction band interact with holes accumulated on the Valence band of MoS_2. through the electron mediator GO sheets. At the same time, es^- from CB of MoS_2 would migrate to VB of Ag_2WO_4. Hence, electrons and holes are effectively separated. The electronic shuttling effect and π-conjunction structure make GO a sink for electrons, Additionally, Graphene oxide having a large surface area acted as efficient support and provided more adsorption sites and catalytic sides for the enhanced degradation process [15]. This may lead to the accumulation of electrons on the CB of MoS_2 and consequently, reduce H^+ to H_2. An abundance of h^+ on VB of silver tungstate causes their accumulation and oxidizes water to O_2.

The increased Photocatalytic activity of AgWMG ternary nanocomposite suggests substantial electron and hole pairs separation. The combination of layered MoS_2 and GO with silver tungstate can provide ample photoelectroactive sites. Besides, the layered structures having specific surface areas can facilitate electron relocation, enhancing visible light-harvesting ability. The introduction of Graphene oxide sheets between MoS_2 and silver tungstate acts as a mediator of electrons migrating at the interface of ternary heterojunction These distinguishing features of ternary heterostructure lead to the improvement of photocatalytic removal of dyes.

7. Antibacterial activity and antibacterial mechanism of ternary nanocomposite

The antibacterial activity of ternary nanocomposite AgWMG and binary AgWG and MG were explored against selected strains of bacteria including both Gram-positive (*Staphylococcus aureus*) and Gram-negative (*Escherichia coli*) strains by disc diffusion method. The bacterial suspensions were made by the cultivation of bacterial strains overnight [46]. Ternary AgWMG with a concentration of 25 mg/ml exhibited maximum activity against all antibacterial strains as compared with binary counterparts which showed very less antibacterial activity. The appearance of a considerable zone of inhibition (mm) around ternary AgWMG predicted good antibacterial activity. The antibacterial effectiveness of ternary and binary samples may be ordered as AgWMG > AgWG > MG. The zones of inhibition produced by ternary samples with 10 mg/ml and 25 mg/ml of concentrations have been illustrated in bar graph Fig. 15. and the images are displayed in the supplementary

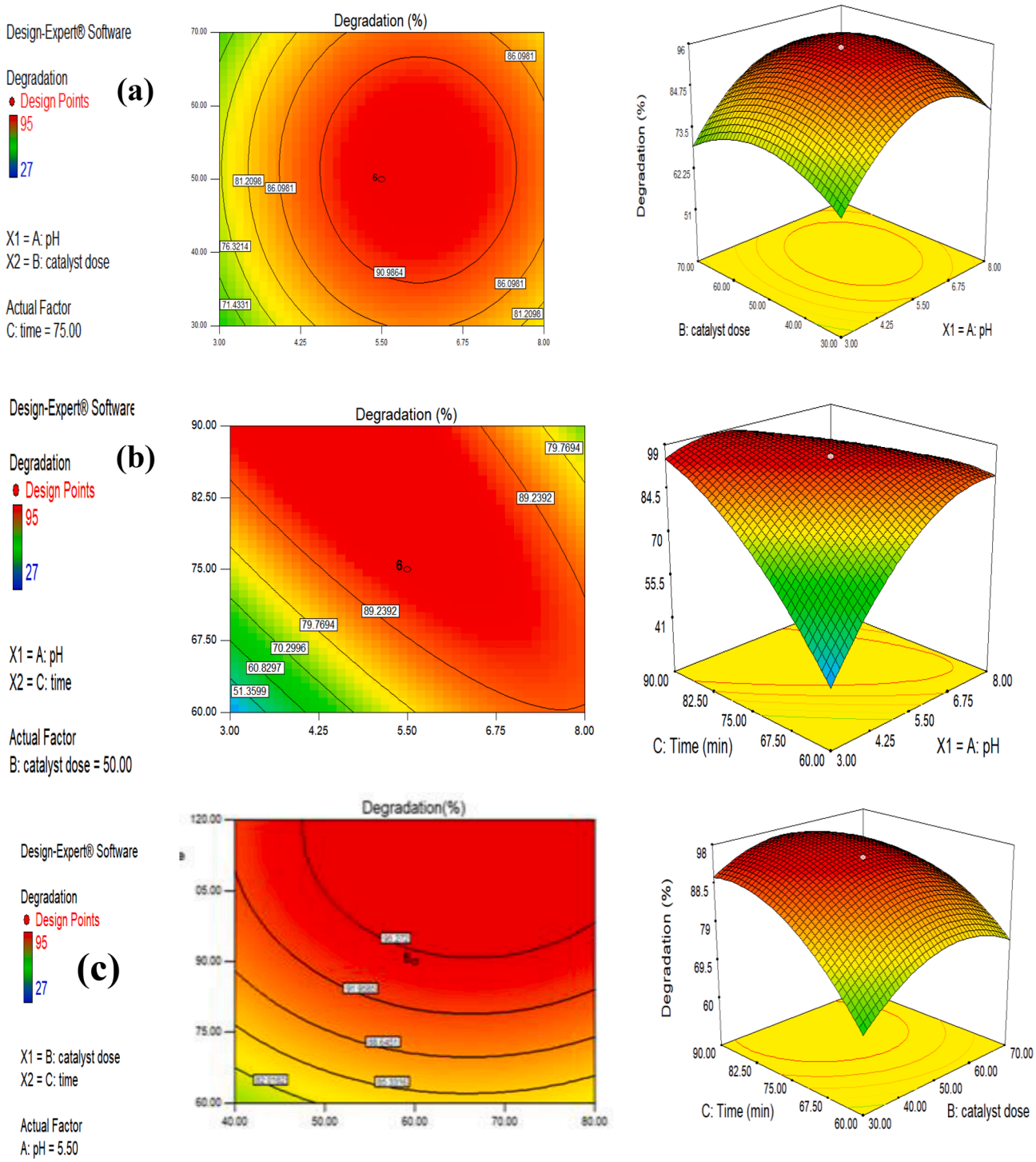

Fig. 12. Response surfaces, displaying the combined effect of (a) pH and, catalyst dose, (b) pH and Time, and (c) catalyst load and, contact time (left side contour plots) (right side, 3D surfaces).

information Fig. S2.

The dissolved oxygen present in water reacts with metal ions and, produces activated oxygen which destroys bacteria. The presence of Ag and W traces owing to their electron trapping ability reduces the recombination of charge carriers leading to improved photocatalytic and antibacterial activity [59].

The three possible mechanisms for the degradation of bacteria by ternary AgWMG may include the generation of reactive species, the release of the ions, or the interaction of nanoparticles with the cell wall [24]. The size and shape of the nanoparticle may also affect bactericidal characteristics. The cytotoxin produced by nanoparticles also causes the inactivation of enzymes in bacteria via ROS production. The hydroxyl radical (•OH) holes (h^+) and, superoxide ($\bullet O^{2-}$) radicals are supposed to have a strong oxidation effect on bacterial cells. Yet, among all these reactive species, which species plays a more significant role in bacterial inactivation remains uncertain. A proposed mechanism has been shown in (Fig. 14). The cell walls of bacteria may be single-layered or multi-layered. Usually, the cell wall of gram-positive bacteria is much more fragile in comparison to gram-negative bacteria against silver tungstate-based nanocomposites [14]. The results shown in the bar graphs depict

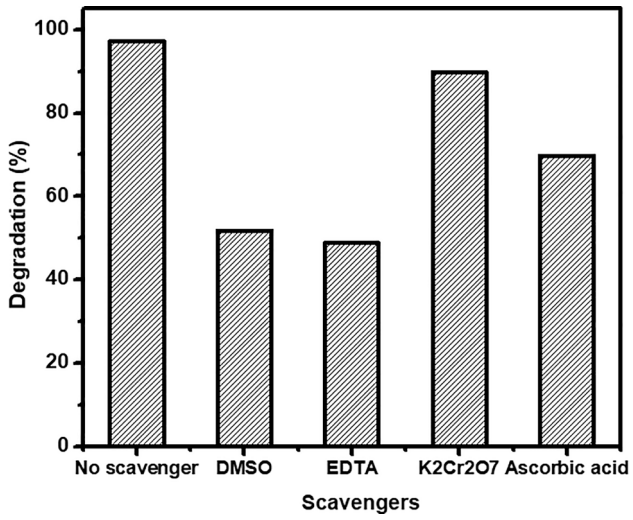

Fig. 13. Scavenging study by ternary AgWMG nanocomposite.

that relative inhibition of *S.aureus* and *E. coli* was higher by ternary AgWMG as compared to binary counterparts. The relative inhibition by ternary AgWMG at 10 mg/ml and 25 mg/ml were 14 and 18 for E.coli and 14 and 26 for S.aureus compared to Control (ciprofloxacin) for E. coli and S.aureus. Increasing the concentration of catalysts may show an enhanced antibacterial effect [16]. It was observed that increasing the nanoparticle concentration improved the anti-bacterial activity [6].

The antibacterial property of Ternary AgWMG may be ascribed to either generation of denser metal ion species (Ag^{2+}, and W^{3+}, Mo^{+2}), shape and size of nanoparticles, or the enhanced surface area due to ternary heterojunction [5 18].

Molybdenum disulphide (MoS_2), is a broadly studied binary metal-sulphide for photocatalysis and antibacterial activity because of its wide range of visible light absorption. But, it usually undergoes photo-corrosion leading to leakage of large amounts of metal ions usually toxic to bacteria. It is hence coupled with stable semi-conductor metal oxides for water disinfection [9]. The polar surfaces present on MoS_2 nanoflowers provide more reactive species [5].

The anti-microbial activity is basically due to the release of metal ions from the surface of nanoparticles. These nanoparticles upon interaction damages the cell membrane and then essential biomolecules. The generation of reactive oxygen species develops a close affinity with thiol groups, directly inhibiting specific enzyme activity and destroying entire cell physiology [19] The improved antibacterial activity of silver tungstate-based catalysts is either due to the direct interaction of these metal ions Ag^{2+}, W^{3+} and Mo^{+2} with bacterial cells or may be due to interaction of sub-ordinate products with them [24]. These positive ions

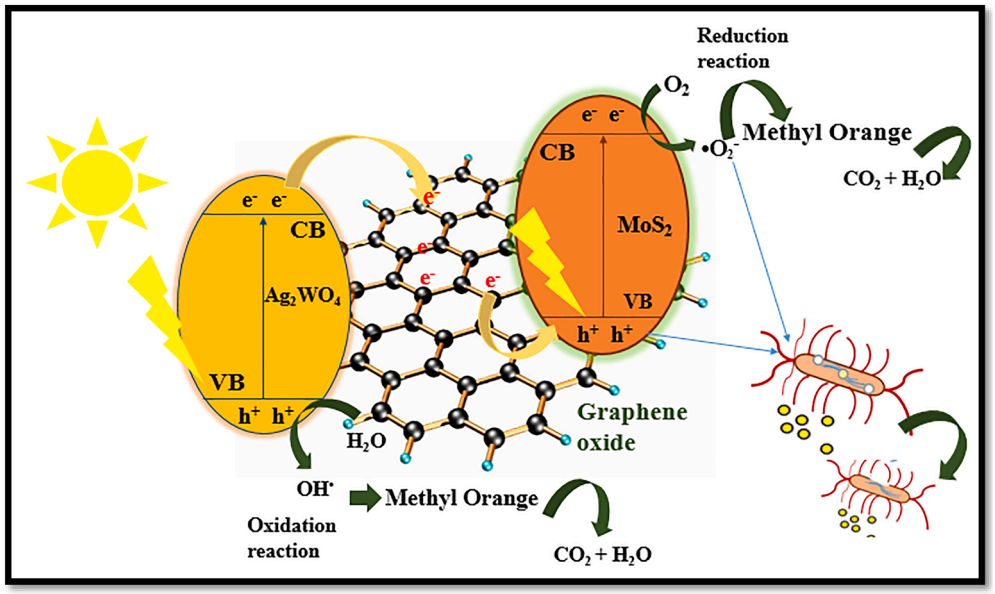

Fig. 14. Proposed MO Photocatalytic degradation and an antibacterial mechanism by ternary AgWMG nanocomposite.

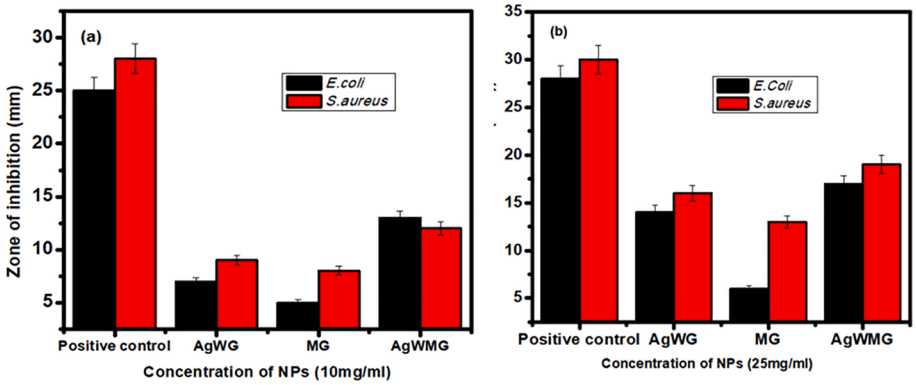

Fig. 15. Zones of inhibition of Ternary and binary nanocomposites against various concentrations.

interact with the negatively charged cell membrane, penetrate and finally attack the sulfhydryl group (-S—H) of the cell membrane. The metallic nanoparticles after penetration into the bacterium reacts with carbonic chains causing lipid peroxidation which leads to DNA molecule dysfunction and protein inactivation [2]. Principally, elements like sulfur (S) nitrogen (N), and phosphorus (P) are replaced interrupting enzymatic production which is vital for micro-organisms. This replacement eventually leads to cell lysis and physiological modification [29].

Moreover, support-based materials like graphene oxide create fertile ground for bacterial inactivation. The improved bacterial inactivation is owing to the enlarged surface area due to support providing active sites in a larger number [58]. The graphene oxide sheets physically wrap around bacterial cells entrapping them potentially. The direct contact between the sharp edges of GO and bacterial cells damages the cell wall and eventually results in intracellular material leakage affecting cell metabolism [8].

8. Conclusion

The present research study has proposed a graphene oxide-supported silver tungstate-based ternary nanocomposite as an effective photocatalyst for environmental remediation utilizing sunlight and also its study as an antibacterial agent. The ternary nanocomposite was successfully designed by an in-situ hydrothermal method and was characterized well using various characterization techniques such as FTIR, XRD, SEM-EDS, TEM, XPS, BET, PL, and UV–vis spectroscopy. The ternary nanocomposite was investigated for its photocatalytic properties for the degradation of methyl orange. In comparison with the binary nanocomposite, the heterogenous ternary hybrid showed enhanced degradation of MO in 90 min at optimized conditions of pH (5), catalyst load (50 mg/100 ml), and IDC (10 ppm). The catalysts also showed improved antibacterial activity against selected strains of bacteria due to the presence of Silver, the small size of ternary nanoparticles, and the greater surface area. The enhanced performance of all nanocomposites was ascribed to the effect of all three individual components and the uniform distribution of MoS_2 and GO sheets. The effective photocatalytic degradation by AgWMG under sunlight and its improved microbial activity suggested that this nanocomposite is a valuable heterostructure material that can be used for a wide range of applications.

Declaration of Competing Interest

The authors declare that they have no known competing financial interests or personal relationships that could have appeared to influence the work reported in this paper.

Data availability

No data was used for the research described in the article.

Acknowledgment

The Open Access funding provided by the Qatar National Library, Doha Qatar. This research was funded by the Higher Education Commission (HEC), Pakistan, under Indigenous 5000 Ph.D. Fellowship with student PIN “pin # 518-121977-2PS5-032 (50043428)”.

Appendix A. Supplementary data

Supplementary data to this article can be found online at https://doi.org/10.1016/j.jphotochem.2022.114376.

References

[1] M.A. Ahmad, S. Aslam, F. Mustafa, U. Arshad, Synergistic antibacterial activity of surfactant free Ag–GO nanocomposites, Sci. Rep. 11 (1) (2021) 1–9.
[2] M. Akter, M.T. Sikder, M.M. Rahman, A.A. Ullah, K.F.B. Hossain, S. Banik, T. Hosokawa, T. Saito, M. Kurasaki, A systematic review on silver nanoparticles-induced cytotoxicity: Physicochemical properties and perspectives, J. Adv. Res. 9 (2018) 1–16.
[3] M. Amiri, M. Salavati-Niasari, A. Pardakhty, M. Ahmadi, A. Akbari, Caffeine: A novel green precursor for synthesis of magnetic CoFe2O4 nanoparticles and pH-sensitive magnetic alginate beads for drug delivery, Materials science and engineering: C 76 (2017) 1085–1093.
[4] H. Ashiq, N. Nadeem, A. Mansha, J. Iqbal, M. Yaseen, M. Zahid, I. Shahid, G-C3N4/Ag@ CoWO4: A novel sunlight active ternary nanocomposite for potential photocatalytic degradation of rhodamine B dye, J. Phys. Chem. Solids 161 (2022), 110437.
[5] G.P. Awasthi, S.P. Adhikari, S. Ko, H.J. Kim, C.H. Park, C.S. Kim, Facile synthesis of ZnO flowers modified graphene like MoS2 sheets for enhanced visible-light-driven photocatalytic activity and antibacterial properties, J. Alloys Compd. 682 (2016) 208–215.
[6] A.T. Babu, M. Sebastian, O. Manaf, R. Antony, Heterostructured nanocomposites of Ag doped Fe3O4 embedded in ZnO for antibacterial applications and catalytic conversion of hazardous wastes, J. Inorg. Organomet. Polym. Mater. 30 (6) (2020) 1944–1955.
[7] A. Balati, A. Bazilio, A. Shahriar, K. Nash, H.J. Shipley, Simultaneous formation of ultra-thin MoSe2 nanosheets, inorganic fullerene-like MoSe2 and MoO3 quantum dots using fast and ecofriendly pulsed laser ablation in liquid followed by microwave treatment, Mater. Sci. Semicond. Process. 99 (2019) 68–77.
[8] L. Behera, B. Barik, S. Mohapatra, Improved photodegradation and antimicrobial activity of hydrothermally synthesized 0.2 Ce-TiO2/RGO under visible light, Colloids and Surfaces A: Physicochemical and Engineering Aspects 620 (2021), 126553.
[9] X. Cao, H. Li, J. He, L. Kang, R. Jiang, F. Shi, H. Xu, Z. Lei, Z.-H. Liu, Preparation and formation process of α-MnS@ MoS2 microcubes with hierarchical core/shell structure, J. Colloid Interface Sci. 507 (2017) 18–26.
[10] L.A. Chanu, W.J. Singh, K.J. Singh, K.N. Devi, Effect of operational parameters on the photocatalytic degradation of Methylene blue dye solution using manganese doped ZnO nanoparticles, Results Phys. 12 (2019) 1230–1237.
[11] A. Chinnathambi, A. Syed, A.M. Elgorban, N. Marraiki, S. Al-Rashed, M.T. Yassin, Performance analysis of novel La6WO12/Ag2WO4 nano-system for efficient visible-light photocatalysis and antimicrobial activity, J. Alloys Compd. 879 (2021), 160075.
[12] F. Davar, M. Salavati-Niasari, Z. Fereshteh, Synthesis and characterization of SnO2 nanoparticles by thermal decomposition of new inorganic precursor, J. Alloys Compd. 496 (1–2) (2010) 638–643.
[13] A. Ebrahimi, N. Jafari, K. Ebrahimpour, M. Karimi, S. Rostamnia, A. Behnami, R. Ghanbari, A. Mohammadi, B. Rahimi, A. Abdolahnejad, A novel ternary heterogeneous TiO2/BiVO4/NaY-Zeolite nanocomposite for photocatalytic degradation of microcystin-leucine arginine (MC-LR) under visible light, Ecotoxicol. Environ. Saf. 210 (2021), 111862.
[14] A.M. Elgorban, A.A. Al Kheraif, A. Syed, Construction of Ag2WO4 decorated CoWO4 nano-heterojunction with recombination delay for enhanced visible light photocatalytic performance and its antibacterial applications, Colloids and Surfaces A: Physicochemical and Engineering Aspects 629 (2021), 127416.
[15] H. Feng W. Zhou X. Zhang S. Zhang B. Liu D. Zhen Synthesis of Z-scheme Mn-CdS/MoS2/TiO2 ternary photocatalysts for high-efficiency sunlight-driven photocatalysis Adv. Compos. Lett. 28 2019 2633366X19895020.
[16] M. Ghiyasiyan-Arani, M. Salavati-Niasari, S. Naseh, Enhanced photodegradation of dye in waste water using iron vanadate nanocomposite; ultrasound-assisted preparation and characterization, Ultrason. Sonochem. 39 (2017) 494–503.
[17] B. Han, Y.H. Hu, MoS2 as a co-catalyst for photocatalytic hydrogen production from water, Energy Sci. Eng. 4 (5) (2016) 285–304.
[18] M. Hasan, J. Iqbal, U. Awan, Y. Saeed, Y. Ranran, Y. Liang, R. Dai, Y. Deng, Mechanistic study of silver nanoparticle's synthesis by dragon's blood resin ethanol extract and antiradiation activity, J. Nanosci. Nanotechnol. 15 (2) (2015) 1320–1326.
[19] M. Hasan, Z. Teng, J. Iqbal, U. Awan, S. Meng, R. Dai, H. Qing, Y. Deng, Assessment of bioreducing and stabilizing potential of Dragon's blood (Dracaena cochinchinensis, Lour. SC Chen) resin extract in synthesis of silver nanoparticles, Nanoscience and Nanotechnology Letters 5 (7) (2013) 780–784.
[20] L.-L. He, X.-P. Liu, Y.-X. Wang, Z.-X. Wang, Y.-J. Yang, Y.-P. Gao, B. Liu, X. Wang, Sonochemical degradation of methyl orange in the presence of Bi2WO6: Effect of operating parameters and the generated reactive oxygen species, Ultrason. Sonochem. 33 (2016) 90–98.
[21] L. Huang, R. Chen, J. Luo, M. Hasan, X. Shu, Synthesis of phytonic silver nanoparticles as bacterial and ATP energy silencer, J. Inorg. Biochem. 231 (2022), 111802.
[22] S. Kokilavani, S.A. Al-Farraj, A.M. Thomas, H.A. El-Serehy, L.L. Raju, S.S. Khan, Enhanced visible light driven photocatalytic and antibacterial activities of Ag2WO4 decorated ZnS nanocomposite, Ceram. Int. 47 (9) (2021) 12997–13006.
[23] S. Kokilavani, A. Syed, H.A. AL-Shwaiman, M.M. Alkhulaifi, F.N. Almajdhi, A. M. Elgorban, S.S. Khan, Preparation of plasmonic CoS/Ag2WO4 nanocomposites: efficient visible light driven photocatalysts and enhanced anti-microbial activity, Colloids Interface Sci. Commun. 42 (2021), 100415.
[24] S. Kokilavani, A. Syed, M.R. Rajeshwari, V. Subhiksha, A.M. Elgorban, A. H. Bahkali, N.S. Zaghloul, A. Das, S.S. Khan, Decoration of Ag2WO4 on plate-like

MnS for mitigating the charge recombination and tuned bandgap for enhanced white light photocatalysis and antibacterial applications, J. Alloys Compd. 889 (2021), 161662.
[25] Kováčová, M. r., Z. M. Marković, P. Humpolíček, M. Micusik, H. Švajdlenková, A. Kleinova, M. Danko, P. Kubat, J. Vajdak and Z. Capakova 2018. Carbon quantum dots modified polyurethane nanocomposite as effective photocatalytic and antibacterial agents. ACS Biomater. Sci. Eng., 4(12): 3983-3993.
[26] K.D. Lakshmi, T.S. Rao, J.S. Padmaja, I.M. Raju, S.A. Alim, P. Kalyani, Visible light driven mesoporous Mn and S co-doped TiO2 nano material: Characterization and applications in photocatalytic degradation of indigocarmine dye and antibacterial activity, Environmental nanotechnology, monitoring & management 10 (2018) 494–504.
[27] S.J. Lee, D.N. Heo, J.-H. Moon, W.-K. Ko, J.B. Lee, M.S. Bae, S.W. Park, J.E. Kim, D. H. Lee, E.-C. Kim, Electrospun chitosan nanofibers with controlled levels of silver nanoparticles. Preparation, characterization and antibacterial activity, Carbohydr. Polym. 111 (2014) 530–537.
[28] M. Liu, X. Xue, S. Yu, X. Wang, X. Hu, H. Tian, H. Chen, W. Zheng, Improving photocatalytic performance from Bi2WO6@ MoS2/graphene hybrids via gradual charge transferred pathway, Sci. Rep. 7 (1) (2017) 1–11.
[29] B. Luo, X. Li, P. Liu, M. Cui, G. Zhou, J. Long, X. Wang, Self-assembled NIR-responsive MoS2@ quaternized chitosan/nanocellulose composite paper for recyclable antibacteria, J. Hazard. Mater. 128896 (2022).
[30] A. Manickavasagan, R. Ramachandran, S.-M. Chen, M. Velluchamy, Ultrasonic assisted fabrication of silver tungstate encrusted polypyrrole nanocomposite for effective photocatalytic and electrocatalytic applications, Ultrason. Sonochem. 64 (2020), 104913.
[31] S. Mirsadeghi, H. Zandavar, M. Yousefi, H.R. Rajabi, S.M. Pourmortazavi, Green-photodegradation of model pharmaceutical contaminations over biogenic Fe3O4/Au nanocomposite and antimicrobial activity, J. Environ. Manage. 270 (2020), 110831.
[32] R. Monsef, M. Salavati-Niasari, M. Masjedi-Arani, Hydrothermal Synthesis of Spinel-Perovskite Li–Mn–Fe–Si Nanocomposites for Electrochemical Hydrogen Storage, Inorg. Chem. 61 (18) (2022) 6750–6763.
[33] S.A. Mosavi, A. Ghadi, P. Gharbani, A. Mehrizad, Photocatalytic removal of Methylene Blue using Ag@ CdSe/Zeoilte nanocomposite under visible light irradiation by Response Surface Methodology, Mater. Chem. Phys. 267 (2021), 124696.
[34] Motaghi, H., P. Arabkhani, M. Parvinnia and A. Asfaram 2021. Simultaneous adsorption of cobalt ions, azo dye, and imidacloprid pesticide on the magnetic chitosan/activated carbon@ UiO-66 bio-nanocomposite: Optimization, mechanisms, regeneration, and application. Sep. Purif. Technol.: 120258.
[35] M. Mousavi, M. Soleimani, M. Hamzehloo, A. Badiei, J.B. Ghasemi, Photocatalytic degradation of different pollutants by the novel gCN-NS/Black-TiO2 heterojunction photocatalyst under visible light: Introducing a photodegradation model and optimization by response surface methodology (RSM), Mater. Chem. Phys. 258 (2021), 123912.
[36] N. Nadeem, Q. Abbas, M. Yaseen, A. Jilani, M. Zahid, J. Iqbal, A. Murtaza, M. Janczarek, T. Jesionowski, Coal fly ash-based copper ferrite nanocomposites as potential heterogeneous photocatalysts for wastewater remediation, Appl. Surf. Sci. 565 (2021), 150542.
[37] B.D. Ossonon, D. Bélanger, Synthesis and characterization of sulfophenyl-functionalized reduced graphene oxide sheets, RSC advances 7 (44) (2017) 27224–27234.
[38] M. Panahi-Kalamuei, S. Alizadeh, M. Mousavi-Kamazani, M. Salavati-Niasari, Synthesis and characterization of CeO2 nanoparticles via hydrothermal route, J. Ind. Eng. Chem. 21 (2015) 1301–1305.
[39] M. Pirhashemi, A. Habibi-Yangjeh, Ultrasonic-assisted preparation of plasmonic ZnO/Ag/Ag2WO4 nanocomposites with high visible-light photocatalytic performance for degradation of organic pollutants, J. Colloid Interface Sci. 491 (2017) 216–229.
[40] A. Rafiq, M. Ikram, S. Ali, F. Niaz, M. Khan, Q. Khan, M. Maqbool, Photocatalytic degradation of dyes using semiconductor photocatalysts to clean industrial water pollution, J. Ind. Eng. Chem. 97 (2021) 111–128.
[41] M.U. Rahman, U.Y. Qazi, T. Hussain, N. Nadeem, M. Zahid, H.N. Bhatti, I. Shahid, Solar driven photocatalytic degradation potential of novel graphitic carbon nitride based nano zero-valent iron doped bismuth ferrite ternary composite, Opt. Mater. 120 (2021), 111408.
[42] A. Raza, M. Ikram, M. Aqeel, M. Imran, A. Ul-Hamid, K.N. Riaz, S. Ali, Enhanced industrial dye degradation using Co doped in chemically exfoliated MoS2 nanosheets, Appl. Nanosci. 10 (5) (2020) 1535–1544.
[43] A. Raza, U. Qumar, J. Hassan, M. Ikram, A. Ul-Hamid, J. Haider, M. Imran, S. Ali, A comparative study of dirac 2D materials, TMDCs and 2D insulators with regard to their structures and photocatalytic/sonophotocatalytic behavior, Appl. Nanosci. 10 (10) (2020) 3875–3899.
[44] M. Rubab, I.A. Bhatti, N. Nadeem, S.A.R. Shah, M. Yaseen, M.Y. Naz, M. Zahid, Synthesis and photocatalytic degradation of rhodamine B using ternary zeolite/WO3/Fe3O4 composite, Nanotechnology 32 (34) (2021), 345705.
[45] M.M.J. Sadiq, U.S. Shenoy, D.K. Bhat, Enhanced photocatalytic performance of N-doped RGO-FeWO4/Fe3O4 ternary nanocomposite in environmental applications, Mater. Today Chem. 4 (2017) 133–141.
[46] M. Shahid I. Naureen M. Riaz F. Anjum H. Fatima M.A. Rafiq Biofilm Inhibition and Antibacterial Potential of Different Varieties of Garlic (Allium sativum) Against Sinusitis Isolates Dose-Response 19 4 2021 15593258211050491.
[47] P. Shandilya, D. Mittal, M. Soni, P. Raizada, A. Hosseini-Bandegharaei, A.K. Saini, P. Singh, Fabrication of fluorine doped graphene and SmVO4 based dispersed and adsorptive photocatalyst for abatement of phenolic compounds from water and bacterial disinfection, J. Clean. Prod. 203 (2018) 386–399.
[48] J. Shen, Y. Lu, J.-K. Liu, X.-H. Yang, Design and preparation of easily recycled Ag2WO4@ ZnO@ Fe3O4 ternary nanocomposites and their highly efficient degradation of antibiotics, J. Mater. Sci. 51 (16) (2016) 7793–7802.
[49] T. Soltani, M.H. Entezari, Photolysis and photocatalysis of methylene blue by ferrite bismuth nanoparticles under sunlight irradiation, J. Mol. Catal. A: Chem. 377 (2013) 197–203.
[50] M.V. Subbaiah, D.-S. Kim, Adsorption of methyl orange from aqueous solution by aminated pumpkin seed powder: Kinetics, isotherms, and thermodynamic studies, Ecotoxicol. Environ. Saf. 128 (2016) 109–117.
[51] A. Sudhaik, P. Raizada, S. Thakur, A.K. Saini, P. Singh, A. Hosseini-Bandegharaei, J.-H. Lim, D.Y. Jeong, V.-H. Nguyen, Peroxymonosulphate-mediated metal-free pesticide photodegradation and bacterial disinfection using well-dispersed graphene oxide supported phosphorus-doped graphitic carbon nitride, Appl. Nanosci. 10 (11) (2020) 4115–4137.
[52] L. Sun, T. Du, C. Hu, J. Chen, J. Lu, Z. Lu, H. Han, Antibacterial activity of graphene oxide/g-C3N4 composite through photocatalytic disinfection under visible light, ACS Sustain. Chem. Eng. 5 (10) (2017) 8693–8701.
[53] A. Tabasum, I.A. Bhatti, N. Nadeem, M. Zahid, Z.A. Rehan, T. Hussain, A. Jilani, Degradation of acetamiprid using graphene-oxide-based metal (Mn and Ni) ferrites as Fenton-like photocatalysts, Water Sci. Technol. 81 (1) (2020) 178–189.
[54] N. Tahir, M. Zahid, I.A. Bhatti, Y. Jamil, Fabrication of visible light active Mn-doped Bi2WO6-GO/MoS2 heterostructure for enhanced photocatalytic degradation of methylene blue, Environ. Sci. Pollut. Res 29 (5) (2022) 6552–6567.
[55] S. Thangavel, S. Thangavel, N. Raghavan, R. Alagu, G. Venugopal, Efficient visible-light photocatalytic and enhanced photocorrosion inhibition of Ag2WO4 decorated MoS2 nanosheets, J. Phys. Chem. Solids 110 (2017) 266–273.
[56] Z. Vaez, V. Javanbakht, Synthesis, characterization and photocatalytic activity of ZSM-5/ZnO nanocomposite modified by Ag nanoparticles for methyl orange degradation, Journal of Photochemistry and Photobiology A: Chemistry 388 (2020), 112064.
[57] J. Wang, J. Xu, X. Wang, H.J. Seo, Morphology modification, spectrum, and optical thermometer application of rare earth ions doped α-Ag2WO4, J. Lumin. 224 (2020), 117303.
[58] W. Wang, G. Huang, C.Y. Jimmy, P.K. Wong, Advances in photocatalytic disinfection of bacteria: development of photocatalysts and mechanisms, Journal of Environmental Sciences 34 (2015) 232–247.
[59] M.F. Warsi, K. Chaudhary, S. Zulfiqar, A. Rahman, I.A. Al Safari, H.M. Zeeshan, P. O. Agboola, M. Shahid, M. Suleman, Copper and silver substituted MnO2 nanostructures with superior photocatalytic and antimicrobial activity, Ceram. Int. 48 (4) (2022) 4930–4939.
[60] J. Xu, X. Lan, J. Cheng, X. Zhou, Facile synthesis of g-C3N4/Ag2C2O4 heterojunction composite membrane with efficient visible light photocatalytic activity for water disinfection, Chemosphere 295 (2022), 133841.
[61] Y. Yang, Z. Wu, R. Yang, Y. Li, X. Liu, L. Zhang, B. Yu, Insights into the mechanism of enhanced photocatalytic dye degradation and antibacterial activity over ternary ZnO/ZnSe/MoSe2 photocatalysts under visible light irradiation, Appl. Surf. Sci. 539 (2021), 148220.
[62] S.R. Yousefi, H.A. Alshamsi, O. Amiri, M. Salavati-Niasari, Synthesis, characterization and application of Co/Co3O4 nanocomposites as an effective photocatalyst for discoloration of organic dye contaminants in wastewater and antibacterial properties, J. Mol. Liq. 337 (2021), 116405.
[63] S.R. Yousefi, O. Amiri, M. Salavati-Niasari, Control sonochemical parameter to prepare pure Zn0. 35Fe2. 65O4 nanostructures and study their photocatalytic activity, Ultrason. Sonochem. 58 (2019), 104619.
[64] A.S. Yusuff, N.B. Ishola, A.O. Gbadamosi, K.A. Thompson-Yusuff, Pumice-supported ZnO-photocatalyzed degradation of organic pollutant in textile effluent: optimization by response surface methodology, artificial neural network, and adaptive neural-fuzzy inference system, Environ. Sci. Pollut. Res 29 (17) (2022) 25138–25156.
[65] B. Zhang, H. Shi, X. Hu, Y. Wang, E. Liu, J. Fan, A novel S-scheme MoS2/CdIn2S4 flower-like heterojunctions with enhanced photocatalytic degradation and H2 evolution activity, J. Phys. D: Appl. Phys. 53 (20) (2020), 205101.
[66] J. Zhang, X. Liu, X. Wang, L. Mu, M. Yuan, B. Liu, H. Shi, Carbon dots-decorated Na2W4O13 composite with WO3 for highly efficient photocatalytic antibacterial activity, J. Hazard. Mater. 359 (2018) 1–8.
[67] H. Zulfiqar, A. Zafar, M.N. Rasheed, Z. Ali, K. Mehmood, A. Mazher, M. Hasan, N. Mahmood, Synthesis of silver nanoparticles using Fagonia cretica and their antimicrobial activities, Nanoscale Advances 1 (5) (2019) 1707–1713.